Electrochemical properties of the [SiW 10 O 36 (M 2 O 2 E 2)] 6– polyoxometalate series (M = Mo(v) or W(v); E = S or O)

Justin Claude Kemmegne-Mbouguen, Sébastien Floquet, Dejin Zang, Antoine Bonnefont, Laurent Ruhlmann, Corine Simonnet-Jégat, Xavier López, Mohamed Haouas, Emmanuel Cadot

New Journal of Chemistry

ARTICLE

Electrochemical properties of the $[SiW_{10}O_{36}(M_2O_2E_2)]^{6-}$ Polyoxometalates series (M = Mo(V) or W(V); E = S or O)

Received 00th January 20xx,
Accepted 00th January 20xx

DOI: 10.1039/x0xx00000x

www.rsc.org/

Justin Claude Kemmegne-Mbouguen,[a,b] Sébastien Floquet,*[,a] Dejin Zang,[c] Antoine Bonnefont,[c] Laurent Ruhlmann,*[,c] Corine Simonnet-Jégat,[a] Xavier López,*[,d] Mohamed Haouas,[a] and Emmanuel Cadot[a]

This paper deals with the electrochemical studies performed in DMF on three iso-structural and iso-electronic compounds of general formula γ–$[SiW_{10}O_{36}(M_2O_2E_2)]^{6-}$, which differ either by the nature of the metallic centers (M = Mo(V) or W(V)) or by the nature of the bridges between Mo(V) atoms (E = O^{2-} or S^{2-}). Interestingly, cyclic voltammetry experiments performed in dry DMF reveal electrochemical processes both in oxidation and in reduction modes. The nature of these processes are studied and elucidated by various electrochemical techniques such as coulometry, rotating disk electrodes, spectro-electrochemistry (IR and UV-Vis), NMR and DFT calculations.

Introduction

Polyoxometalate (POM) compounds, often described as soluble discrete metal-oxide frameworks, can be finely tuned at the molecular level and constitute a wide family rich of more than several thousand inorganic compounds displaying various properties in supramolecular chemistry,[1-3] medicine,[4, 5] magnetism,[6, 7] catalysis[8-10] or electro-catalysis.[11] In this domain, due to their ability for electron storage, POMs constitute very efficient electrocatalysts for reactions of environmental interest such as CO_2 reduction[12] or proton reduction into hydrogen[13-15] and the electro-catalytic reduction and/or detection of environmental pollutants like nitrogen oxides,[16, 17] bromates[18, 19] or iodates.[19-21] Pushed to their maximum of reduction they can also constitute some excellent molecular battery components or molecular capacitors as exemplified for the Keggin structure $[PMo_{12}O_{40}]^{3-}$, which can be reduced by 24 electrons with the formation of Mo-Mo bonds.[22, 23] Based on the fact that sulfide ions are generally invoked for stabilizing lower oxidation states (+V, +IV and +III) of Mo or W atoms,[24, 25] incorporation of Mo-S or W-S clusters in the POM framework is expected to modify their electronic properties and therefore their electro-catalytic properties. A fruitful approach for the syntheses for sulfur-containing POMs was developed by reacting the electrophilic $\{Mo_2O_2S_2\}^{2+}$ or $\{Mo_3S_4\}^{4+}$ cores with vacant polyoxotungstate ions.[26-28] Regarding the potentialities of the method and the growing interest for such compounds, this field of investigation continues to be one of our main focuses and some spectacular compounds have been obtained by following this strategy.[26, 27, 29] However, the domain of S-containing POMs has been for long time neglected and the literature describing the electrochemical properties of such S-containing POMs is consequently very poor, while coordination complexes based on $\{Mo_2O_xS_y\}^{2+}$ ($x + y = 4$) core have been widely studied in the 1970s and the 1980s[25, 30, 31] and despite that $\{Mo_2O_2S_2\}^{2+}$ or $\{Mo_3S_4\}^{4+}$ based compounds exhibit very interesting properties for electro-catalytic reduction of protons into hydrogen in organic or in aqueous media.[32-40]

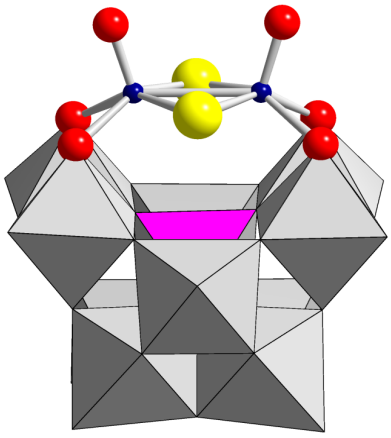

Figure 1. Structure of compounds $[SiW_{10}O_{36}(M_2O_2E_2)]^{6-}$ used in this study with M = Mo or W (blue spheres) and E = O or S (yellow spheres). Oxygen atoms are depicted in red, WO_6 and SiO_4 octahedra are given in grey and in pink respectively.

[a] Institut Lavoisier de Versailles, UVSQ, CNRS, Université Paris-Saclay, 45 avenue des Etats-Unis, 78035 Versailles Cedex, France. E-mail: sebastien.floquet@uvsq.fr.
[b] Laboratoire de Chimie Analytique, Faculté des Sciences, Université de Yaoundé I,B.P. 812, Yaoundé, Cameroon. E-mail: jkemmeg@yahoo.fr
[c] Laboratoire d'Electrochimie et de Chimie Physique du Corps Solide, Institut de Chimie-UMR 7177, C.N.R.S., Université de Strasbourg, 4 rue Blaise Pascal, 67081 Strasbourg Cedex, France. E-mail: lruhlmann@unistra.fr.
[d] Universitat Rovira i Virgili, Departament de Química Física i Inorgànica, Tarragona, Spain. E-mail: javier.lopez@urv.cat

Electronic Supplementary Information (ESI) available: FT-IR spectra of the compounds used in this study (Figure S1); Additional electrochemical data (Figure S2-S6), additional UV-Vis-NIR spectroelectrochemistry experiments (Figure S7-S12); effect of addition of an excess of Br_2 on the electronic spectra of **$\{SiW_{10}Mo_2O_2S_2\}$** in DMF (Figure S13); ^{29}Si NMR spectra of **$\{SiW_{10}Mo_2O_2S_2\}$** in DMF/CH_3CN mixtures before and after addition of one equivalent of Br_2 (Figure S14). See DOI: 10.1039/x0xx00000x

In this contribution, we focus on three compounds resulting from the combination of the divacant POM γ-$[SiW_{10}O_{36}]^{8-}$ (denoted hereafter SiW_{10}) with three different cationic building blocks, i.e. $[Mo^{V}_{2}O_2S_2]^{2+}$, $[W^{V}_{2}O_2S_2]^{2+}$ and $[Mo^{V}_{2}O_4]^{2+}$ (see Figure 1).[41, 42] These three compounds are well known since long time but, to our knowledge, their electrochemical properties have not been reported yet. The aims of this work are to bring new insights about the effects of the introduction of sulfurated clusters in POM architectures and also to study the breaking and the reformation and of the M-M bonds in the three $[M^{V}_{2}O_2E_2]^{2+}$ clusters associated to the oxidation/reduction processes localized on the M atoms. We present therefore the electrochemical studies performed in DMF on the three electronic compounds $[SiW_{10}O_{36}(M_2O_2E_2)]^{6-}$ (M = Mo or W; E = S or O), which differ either by the nature of the metallic centers (Mo(V) or W(V)) or by the nature of their bridging groups (O^{2-} or S^{2-}). For confident interpretation of the redox processes involved for these three compounds, these studies are supported by spectro-electrochemical studies, DFT calculations and NMR studies.

Results and discussion

Electrochemical properties of $\{SiW_{10}\text{-}Mo_2O_4\}$, $\{SiW_{10}\text{-}Mo_2O_2S_2\}$, and $\{SiW_{10}\text{-}W_2O_2S_2\}$ in dry DMF.

Cyclic voltammetry, Rotating Disk Voltammetry and Coulometry.

Electrochemical properties of **$\{SiW_{10}\text{-}Mo_2O_4\}$**, **$\{SiW_{10}\text{-}Mo_2O_2S_2\}$**, and **$\{SiW_{10}\text{-}W_2O_2S_2\}$** were investigated in DMF by cyclic voltammetry and rotating disk voltammetry (RDV). Redox potentials, the separation between the anodic and the cathodic peaks of the redox processes (ΔE_p) as well as the number of electron exchanged are gathered in Table 1. Figure 2 compares cyclic voltammograms obtained for the three compounds with a scan rate of 100 $mV.s^{-1}$ over the potential range +0.5 to –1.6 V *vs.* SCE in dry DMF containing 0.1 M $LiClO_4$ as the supporting electrolyte, while Figure 3 focuses on the cyclic and the rotating electrode voltamograms obtained for **$\{SiW_{10}\text{-}Mo_2O_4\}$** (0.3 mM). As depicted in Figure 3A (curve a), on the first potential sweep of CV, two successive one-electron reversible reductions at E = –1.112 V (process I_a) and E = –1.179 V (process I_b ; $I_a/I_c \approx 1$ for processes I_a and I_b; ΔE_p = 87 and 85 mV, respectively) and one two electron oxidation process at E = –0.204 V (process II) are observed. In addition, the global cathodic processes I_a and I_b of the reduction are almost proportional to the square root of the scan rate from 100 to 1000 $mV.s^{-1}$ (see Figure S2, Supporting Information), which indicates that electron exchanges are diffusion-controlled.

In the case of the oxidation process II at –0.204 V, the difference between cathodic and anodic potentials (ΔE_p) is 297 mV, more than 58.5/*n* mV (*n* = number of exchanged electrons) expected for reversible process, showing slow reversible process for wave II. On repetitive potential cycling or for the reverse sweep, the reversible processes I and II remained unchanged.

In the same conditions, using rotating disk electrode, two well resolved waves with equal limiting current were also observed corresponding to processes I (I_a + I_b) and II (Figure 3B). Furthermore, the half wave potential or $E_{1/2}$ value calculated from the potential when the current has the half value of the limiting current I_{Lim} are the same as redox potential value determined from cyclic voltammetry for process II. Strikingly, the position of the zero current lies exactly between redox processes I and II, suggesting that the compound is oxidized during process II and gives rise to a positive current, and is reduced and exhibits a negative current for process I. These two well resolved waves with nearly equal limiting current for both processes I and II indicate that the same number of electrons is involved in these processes.

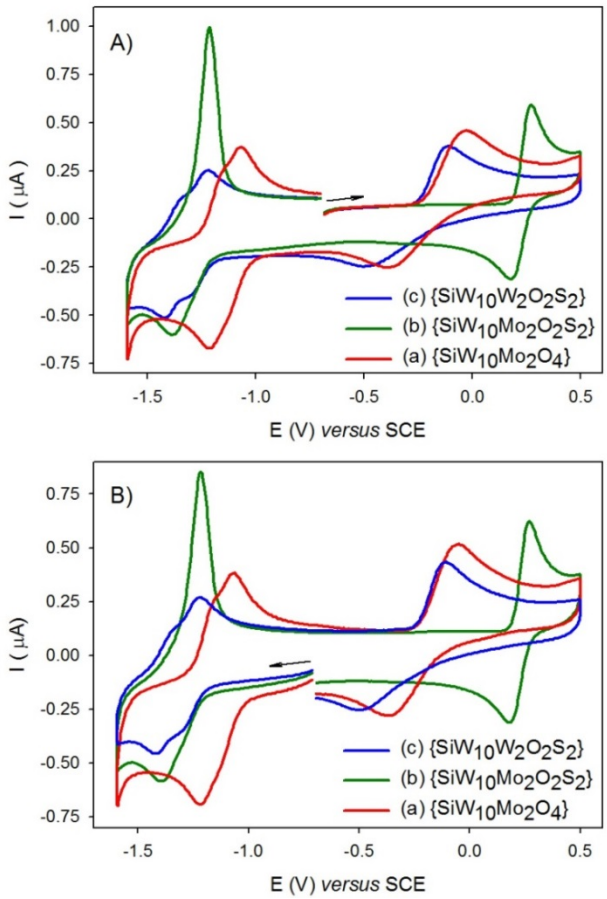

Figure 2 Cyclic voltammograms at a glassy carbon electrode (v = 0.1 V s^{-1}) for 0.3 mM solutions of the three compounds **$\{SiW_{10}\text{-}Mo_2O_4\}$** (a), **$\{SiW_{10}\text{-}Mo_2O_2S_2\}$** (b), and **$\{SiW_{10}\text{-}W_2O_2S_2\}$** (c) in dry DMF 0.1 M $LiClO_4$ as the supporting electrolyte. (A) Cycles starting towards the oxidation processes; (B) Cycles starting towards the reduction processes

Table 1. Cyclic voltammetry and rotating disk voltammetry data recorded in DMF 0.1 M $LiClO_4$ of **$\{SiW_{10}\text{-}Mo_2O_4\}$** (a), **$\{SiW_{10}\text{-}Mo_2O_2S_2\}$** (b), and **$\{SiW_{10}\text{-}W_2O_2S_2\}$** (c).

Species	Cyclic voltammetry			
	$E°$ [V][i]	Process	ΔE_p [mV][ii]	E_p [V][iii]
$\{SiW_{10}\text{-}Mo_2O_4\}$	–0.204 (2 e^-)	II	297	
(a)	–1.112 (1 e^-)	I_a	87	
	–1.179 (1 e^-)	I_b	85	
$\{SiW_{10}\text{-}Mo_2O_2S_2\}$		III		+0.877
(b)	+0.226 (2 e^-)[iv]	II	81	
	–1.302 (2 e^-)	I	170	
$\{SiW_{10}\text{-}W_2O_2S_2\}$	–0.297(2 e^-)	II	347	
(c)	–1.257 (1 e^-)	I_a	70	
	–1.372 (1 e^-)	I_b	75	

[i] $E° = (E_{pc} + E_{pa})/2$, where E_{pc} and E_{pa} correspond to the cathodic and anodic peak potentials, respectively. [ii] $\Delta E_p = E_{pa} - E_{pc}$. [iii] irreversible. [iv] Two electrons exchanged from the CV and the RDV and 4 electrons exchanged from the exhaustive coulometry at applied potential of +0.300 V *vs.* SCE.

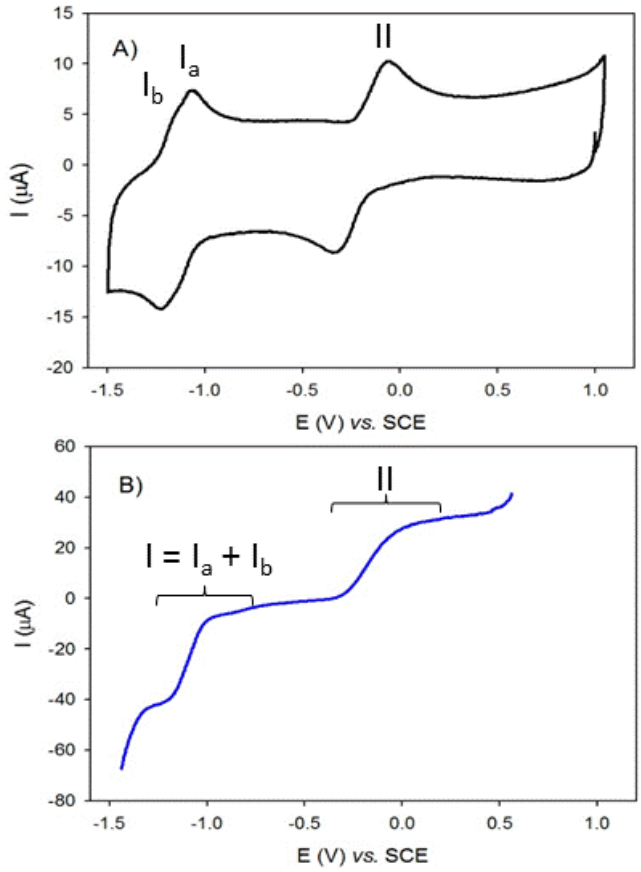

Figure 3 Cyclic (A) and RDE (B) voltammograms at a glassy carbon electrode (v = 0.1 V s^{-1}) for 0.3 mM **{SiW_{10}-Mo_2O_4}** in dry DMF containing 0.1 M $LiClO_4$ as the supporting electrolyte (for RDE ω = 1000 rpm, v = 0.01 V s^{-1}).

Controlled-potential coulometry was conducted for **{SiW_{10}-Mo_2O_4}** after process I at –1.42 V. It was found that process I exchanged 1.9 electrons *per* anion (one electron for each I_a and I_b processes which cannot be observed separately), which indicates that waves I and II are two-electron processes. Consequently, process II is attributed to the oxidation of the two Mo(V) centers of the $[Mo_2O_4]^{2+}$ moiety of **{SiW_{10}-Mo_2O_4}** into Mo(VI) with the breaking of the Mo^V-Mo^V bond to give the compound $[SiW_{10}O_{36}(Mo^{VI}{}_2O_4)]^{4-}$ already reported by Tézé et al.,[41] whereas processes I_a and I_b are assigned to the reduction of two W(VI) atoms of the SiW_{10} moiety into W(V), even if the reduction of $\{Mo_2O_xS_y\}^{2+}$ ($x + y = 4$) core can occurs in this region in aqueous or in non-aqueous solvent when associated with organic ligands.[25, 30, 31]

The CV of polyoxothiometalate counterparts **{SiW_{10}-$Mo_2O_2S_2$}** and **{SiW_{10}-$W_2O_2S_2$}** are shown in Figure 2 (curves b and c, respectively) as well as in Figures S2-S6 in Supporting Information. Both of them exhibit similar redox behavior to that of **{SiW_{10}-Mo_2O_4}** showing two very close reversible processes at negative potential (processes I_a and I_b) and one two electrons oxidation process at more positive potential (process II). Furthermore, as for **{SiW_{10}-Mo_2O_4}**, the cathodic peaks of the first reduction (process I) are almost proportional to the square root of the scan rate from 100 to 1000 mVs^{-1} (see Figures S2-S3, and Figure S6, Supporting Information), which indicated that electron-exchange are diffusion-controlled. In contrast to **{SiW_{10}-Mo_2O_4}**, the sulfurated compound **{SiW_{10}-$Mo_2O_2S_2$}** showed at more negative potential a sharp anodic peak potential observed at E_{pa} = –1.302 V, typical to the peak of redissolution of an adsorbed reduced compound (see Figure 2, curve b and Figures S3-S5 in Supporting Information). This observation indicated that the reduced species possesses a high affinity for the glassy carbon in dry DMF and remained adsorbed on the surface of the glassy carbon electrode. This adsorption is characteristic of sulfurated clusters like Mo_2S_2 cores present in polyoxothiometalates **{SiW_{10}-$Mo_2O_2S_2$}**, and **{SiW_{10}-$W_2O_2S_2$}**.[43] In contrast, in the case of the sulfurated compound **{SiW_{10}-$W_2O_2S_2$}**, analogous redox behavior in reduction was observed. The two successive reversible reduction processes at E = –1.257 V and E = –1.372 V correspond to one-electron processes.

Compared to **{SiW_{10}-Mo_2O_4}**, the first reduction wave corresponding to the reduction of the SiW_{10} part is negatively shifted about 190 and 145 mV for **{SiW_{10}-$Mo_2O_2S_2$}**, and **{SiW_{10}-$W_2O_2S_2$}**, respectively, highlighting the relatively strong effect of the sulfurated fragment on the properties of the POM moiety. Due to the formation of deposits on the electrode surface, it was not possible to confidently perform coulometry in reduction mode in the case of **{SiW_{10}-$Mo_2O_2S_2$}**, but in comparison with **{SiW_{10}-Mo_2O_4}** we can reasonably suppose that this reduction process I exchange two electrons and thus corresponds to the reduction of two W^{VI} atoms of the SiW_{10} into W^V. In the case of **{SiW_{10}-$W_2O_2S_2$}** controlled-potential coulometry was conducted after processes I_a and I_b showing the exchanged 2.0 electrons *per* molecule for the global reduction process I.

For the waves corresponding to the oxidation of Mo(V) of Mo_2O_4 cluster in **{SiW_{10}-Mo_2O_4}**, the latter are less affected for **{SiW_{10}-$Mo_2O_2S_2$}**, than for **{SiW_{10}-$W_2O_2S_2$}** which confirm that this oxidation can be assigned to the clusters coordinated to the SiW_{10} moiety. In comparison with **{SiW_{10}-Mo_2O_4}**, the potential is negatively shifted by about 93 mV in the case of **{SiW_{10}-$W_2O_2S_2$}**. The replacement of the $\{Mo_2O_4\}$ core by $\{Mo_2O_2S_2\}$ results in a much stronger modification since the potential is up-shifted by about 430 mV. Interestingly the oxidation wave is rapid and reversible at a scan rate of 100 mV s^{-1} for **{SiW_{10}-$Mo_2O_2S_2$}** (ΔE_p = 81 mV) while numerous $\{Mo_2O_2S_2\}$-based cyclic compounds or coordination complexes usually exhibit irreversible oxidation wave in organic medium,[25, 33, 34, 36] which suggests that the SiW_{10} POM moiety, which plays the role of inorganic rigid ligand, probably stabilizes the oxidized form of this cluster. Similarly to the two previous compounds, this wave was first assigned to the oxidation of the two Mo(V) atoms of the $\{Mo_2O_2S_2\}$ core into Mo(VI) with the breaking of the Mo-Mo bond and these results are in agreement with the stabilization of lower oxidation states, here Mo(V), by sulfides.[25]

Controlled-potential coulometry at applied potential of +0.345 V *vs.* SCE of **{SiW_{10}-$Mo_2O_2S_2$}** indicated the exchange of 3.9 electrons per anion while only 2 electrons were expected to be observed from the cyclic voltammogram and the rotating disk voltammogram. This discrepancy and the exchange of 2 electrons more than for **{SiW_{10}-Mo_2O_4}** could be explained first by the different time scales of the experiments: less than one minute for the cyclic voltammetry (CV) *versus* several hours for the coulometry. However, in order to have twice more electrons exchanged per molecule, it might be suggested that both the oxidation of the two Mo(V) to Mo(VI) (2 first electrons exchanged) were followed by the oxidation of the two bridging sulfides of the $\{Mo_2O_2S_2\}$ core for forming a disulfide bridge. As shown in Figure S3A (Supporting Information), cyclic voltammetry performed at higher potential exhibits an irreversible

wave around 0.9 V, which could be assigned to the direct oxidation of sulfides.

Question thus arises to unambiguously assign the origin of the reversible wave observed at + 0.226 V *vs.* SCE for **{SiW$_{10}$-Mo$_2$O$_2$S$_2$}**. Starting from the core depicted in Scheme 1 with two Mo(V) atoms linked by a Mo-Mo bond and two bridging sulfides, spectroscopic characterization and DFT calculations were performed to elucidate its oxidation process: oxidation of Mo(V) into Mo(VI) with the breaking of the Mo-Mo bond or oxidation of the two bridging sulfides to give a bridging disulfide ligand between two Mo(V) atoms, a configuration rarely reported in the literature for Mo^{V}-S clusters, or something else.

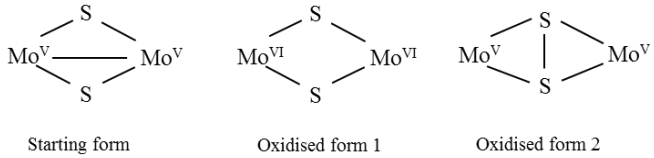

Scheme 1

Spectroelectrochemical investigations.

To gain further insights into the nature of the electrogenerated species, *in-situ* UV-Vis-NIR spectroelectrochemical and *in-situ* NIR spectroelectrochemical studies have been carried out on **{SiW$_{10}$-Mo$_2$O$_4$}**, **{SiW$_{10}$-Mo$_2$O$_2$S$_2$}** and **{SiW$_{10}$-W$_2$O$_2$S$_2$}** in DMF solution containing 0.1 mol L^{-1} $LiClO_4$ as the electrolyte (Figures 4 and 6, and Figures S7-S13 in SI).

{SiW$_{10}$-Mo$_2$O$_4$}, **{SiW$_{10}$-Mo$_2$O$_2$S$_2$}** and **{SiW$_{10}$-W$_2$O$_2$S$_2$}** are spectrally characterized by oxygen-to-tungsten and oxygen-to-molybdenum charge transfer (O–W and O-Mo CT) bands in the UV spectral domain (λ < 380 nm) and have much weaker absorption band in the visible region in the 400-480 nm range assigned to the charge transfer between bridging oxo or sulfido ligands to Mo^{V} or W^{V} centers of the $[M_2O_2E_2]^{2+}$ fragment.[42]

In the case of **{SiW$_{10}$-Mo$_2$O$_4$}** in DMF, *in-situ* UV-Vis-NIR spectroelectrochemical studies at applied potential of –1.420 V *vs.* SCE are shown in Figure 4A and Figure S7 (SI). Several large bands between 550 nm to 1900 nm increased moderately with the concomitant decrease of intensity of the O–W CT band near 280 nm. Consequently, the reduced form exhibit moderate broad absorption bands around 550–1900 nm attributed to d–d transitions and tungsten-to-tungsten intervalence charge transfer (W^{5+}–W^{6+} IVCT). The reduced form also presented a decrease in the initial O–W CT bands (at λ < 380 nm, Figure 4). These results indicate that the reduction process probably corresponds to the reduction of two W(VI) atoms to form W(V), as previously proposed.

In-situ UV-Vis-NIR spectroelectrochemical studies for the oxidation of **{SiW$_{10}$-Mo$_2$O$_4$}** at applied potential of +0.345 V *vs*. SCE showed vanishing of the small band near 400 nm and the moderate increase of the bands at 350 and 280 nm (Figures 4B and Figure S8 in SI). The small band near 400 nm is probably associated to oxygen-to-molybdenum (V) charge transfer (O–Mo(V) CT) bands.[41, 42] Upon the oxidation of the two Mo(V) to Mo(VI), this band disappeared confirming the formation of the colorless compound $[SiW_{10}O_{36}(Mo^{VI}{}_2O_4)]^{4-}$.[41]

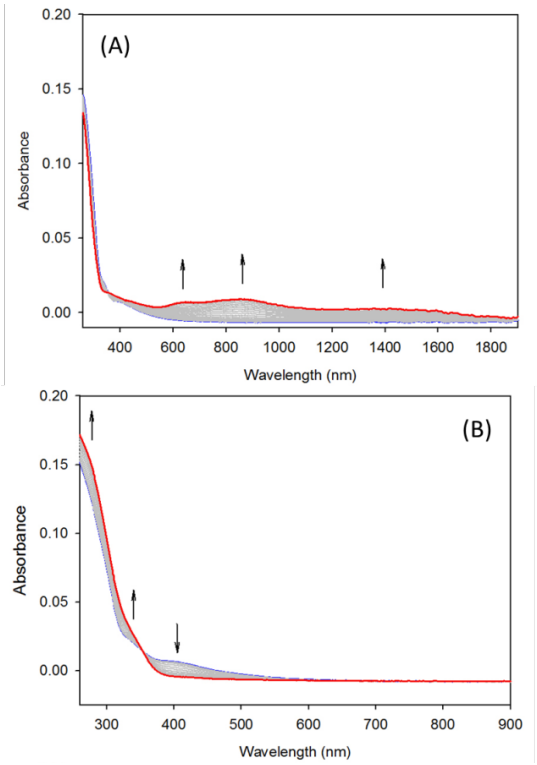

Figure 4. UV-Vis-NIR spectroelectrochemistry within Room Temperature OTTLE recorded during reduction or oxidation of **{SiW$_{10}$-Mo$_2$O$_4$}** (c = 0.1 mM) in DMF + 0.1 M $LiClO_4$. (A) Absorbance measurements during reduction at −1.420 V *vs.* SCE; (B) Absorbance measurements during oxidation at +0.345 V *vs.* SCE.

In the case of **{SiW$_{10}$-Mo$_2$O$_2$S$_2$}**, *in-situ* UV-Vis-NIR spectroelectrochemical studies of reduction were very difficult because of the strong adsorption of the reduced compound onto the surface of the platinum electrode as already observed for the cyclic voltammetry studies. Nevertheless, as for **{SiW$_{10}$-Mo$_2$O$_4$}**, the reduction at applied potential of –1.450 V *vs*. SCE led to the formation of large bands in the visible and NIR region between 550 and 1900 nm (Figure S9, SI), suggesting also the reduction of two W(VI) to W(V) atoms. This reduced form exhibit broad absorption bands around 550–1900 nm attributed to d–d transitions and tungsten-to-tungsten intervalence charge transfer (W^{5+}–W^{6+} IVCT). The reduced form also presented a decrease in the O–W CT bands as observed for **{SiW$_{10}$-Mo$_2$O$_4$}**. It must be remarked that the slight change of the bands' intensities during the reduction was due to the strong adsorption of the reduced compound onto the Pt grid electrode. *In-situ* UV-Vis-NIR spectroelectrochemical studies for the oxidation of **{SiW$_{10}$-Mo$_2$O$_2$S$_2$}** at +0.380 V *vs.* SCE presented different behavior compared to **{SiW$_{10}$-Mo$_2$O$_4$}** (Figure S10, SI). In this case, we observed only a little change of the spectra: small increase of the intensity of the bands at 280 and 350 nm and the formation of two new bands near 490 and 600 nm, which could correspond only to a partial oxidation of the Mo^{V} centers of the $[Mo_2O_2S_2]^{2+}$ fragment.

Direct chemical oxidation of **{SiW$_{10}$-Mo$_2$O$_2$S$_2$}** by Br_2 in DMF/CH_3CN mixture was therefore performed and followed by UV-Visible spectroscopy (Figure S13, SI) and NMR (Figure 5 and Figure S14, SI). In contrast with *In-situ* UV-Vis-NIR spectroelectrochemical studies, the stepwise addition of Br_2 up to 2.5 equivalents of Br_2 per {SiW_{10}-$Mo_2O_2S_2$} leads to the total disappearance of the oxygen-to-

molybdenum(V) charge transfer (O–Mo(V) CT) band in agreement with the oxidation of Mo(V) into Mo(VI). Furthermore, as shown in Figure 5 and in Figure S13 (SI), the addition of only one equivalent of Br_2 to $\{SiW_{10}\text{-}Mo_2O_2S_2\}$ in DMF/CH_3CN mixture (2/1 ratio in volume) gives strong modification in ^{183}W and ^{29}Si NMR spectra. $\{SiW_{10}\text{-}Mo_2O_2S_2\}$ gives one unique signal in ^{29}Si NMR (Figure S14, SI) and three NMR lines in ^{183}W NMR (Figure 5) with relative intensities 4/4/2 in agreement with the ten tungsten atoms involved in the C_{2v} structure of $\{SiW_{10}\text{-}Mo_2O_2S_2\}$ (see Figure 1). This result is in perfect agreement with the spectrum published by Cadot et al.[42] By addition of one equivalent of Br_2, a part of the starting compound remains non-oxidized, while three new sharp lines in ^{183}W NMR appear at –113.0, –103.3 and –129.8 ppm. The latter are unambiguously attributed to the fully oxidized oxo compound $[SiW_{10}O_{36}(Mo^{VI}{}_2O_4)]^{4-}$.[41] This result indicates both the oxidation of Mo(V) into Mo(VI) and the oxidation of sulfides, probably into elemental sulfur, which are removed from the compound. The ^{29}Si NMR is in agreement with ^{183}W NMR experiments showing the presence of the starting signal together with one more signal assigned to $[SiW_{10}O_{36}(Mo^{VI}{}_2O_4)]^{4-}$.[41] Furthermore, additional broad signals are observed in ^{29}Si and in ^{183}W, which correspond to some unknown degradation products. In summary, direct chemical oxidation by a strong non-selective oxidant like Br_2 evidenced that both oxidation of sulfide and Mo(V) atoms are possible.

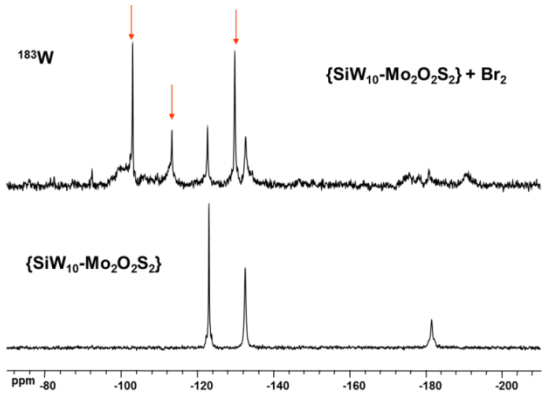

Figure 5. ^{183}W NMR spectra of **$\{SiW_{10}\text{-}Mo_2O_2S_2\}$** in DMF/$CH_3CN$ (2/1 ratio in volumes) before and after addition of one equivalent of Br_2. The red arrows indicate the lines assigned to the oxidized compound $[SiW_{10}O_{36}(Mo^{VI}{}_2O_4)]^{4-}$.

Similar behavior has been obtained in the case of **$\{SiW_{10}\text{-}W_2O_2S_2\}$** as shown in Figures S11-S12 for *in-situ* UV-Vis-NIR spectroelectrochemical studies of reduction at –1.500 V *vs.* SCE (Figure S11, SI) or for oxidation at +0.345 V *vs.* SCE (Figure S12, SI).

In the 600-1100 cm^{-1} range, the FT-IR spectra of **$\{SiW_{10}\text{-}Mo_2O_4\}$**, **$\{SiW_{10}\text{-}Mo_2O_2S_2\}$** and **$\{SiW_{10}\text{-}W_2O_2S_2\}$** exhibit different strong vibration bands assigned both to M^V=O vibrations of the $[M_2O_2E_2]^{2+}$ cluster and W^{VI}=O vibrations of the POM part in the 900-980 cm^{-1} range and different kinds of ν_{as}-(W-O-W) absorptions of the SiW_{10} moiety from 740 to 900 cm^{-1} (Figure 6 and Figure S1 in SI).[41, 42, 44, 45]

In-situ IR spectroelectrochemical studies for the oxidation of **{$\{SiW_{10}\text{-}Mo_2O_4\}$**, **$\{SiW_{10}\text{-}Mo_2O_2S_2\}$** and **$\{SiW_{10}\text{-}W_2O_2S_2\}$** have been performed in the same media at applied potential of +0.345 V *vs.* SCE (Figure 6). It is noteworthy that the IR spectra are recorded in solution and can differ significantly from those recorded in ATR mode or in KBr pellet in terms of intensities and to a lesser extent of position. For the three compounds, the evolution of the IR spectra during the electrolysis exhibits isobestic points (not shown) which translate by an equilibrium between two species in solution. In the region 1100–600 cm^{-1}, for the three compounds the evolutions of the FT-IR spectra display significant modification of the M=O absorption bands, whereas the (W-O-W) region is much less affected in the case of **$\{SiW_{10}\text{-}Mo_2O_4\}$** and **$\{SiW_{10}\text{-}Mo_2O_2S_2\}$**. For **$\{SiW_{10}\text{-}Mo_2O_4\}$** the peaks at 899 and 954 cm^{-1} are shifted from 14 cm^{-1} to 912 and 968 cm^{-1}, respectively. This shift of the wavenumbers is less pronounced for **$\{SiW_{10}\text{-}Mo_2O_2S_2\}$** and **$\{SiW_{10}\text{-}W_2O_2S_2\}$** (8-10 cm^{-1}). These two absorptions are attributed to the elongation vibrations of the terminal Mo=O or W=O bonds in the $[M_2O_2S_2]^{2+}$ fragment and the terminal W=O bonds of the SiW_{10} moiety. The increasing of the wavenumber of the M=O vibrations for 8-14 cm^{-1} is in agreement with the oxidation of the Mo(V) or W(V) atoms into Mo(VI) or W(VI), while the vibrations of the W=O bonds of the SiW_{10} part are also affected by the decreasing of the global charge of the compounds and thus the variation of electronic density on the terminal oxo ligands on which the charge is distributed. Finally, in contrast with **$\{SiW_{10}\text{-}Mo_2O_4\}$** and **$\{SiW_{10}\text{-}Mo_2O_2S_2\}$**, the W-O-W vibrations in **$\{SiW_{10}\text{-}W_2O_2S_2\}$** are also modified after oxidation at applied potential of +0.345 V *vs.* SCE (Figure 6C) accordingly to the creation of new W-O-W fragment upon oxidation of the W^V into W^{VI}.

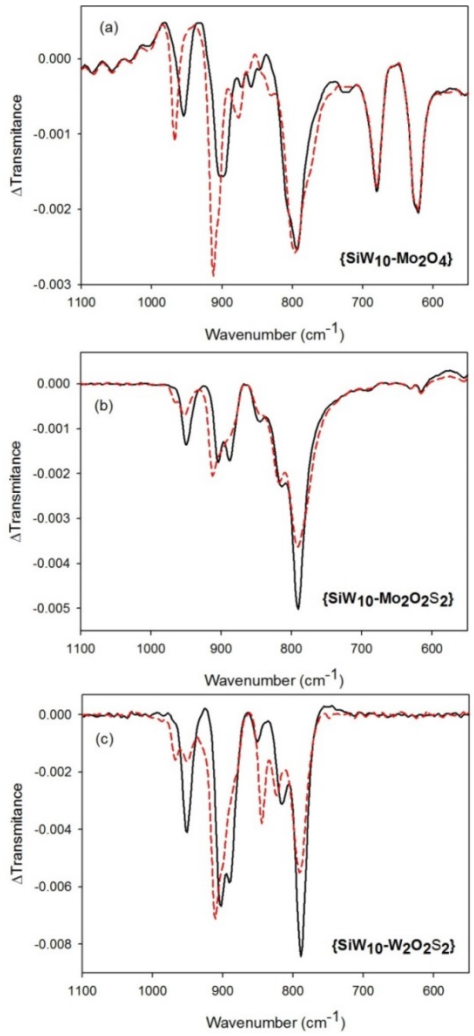

Figure 6. IR spectroelectrochemistry in room temperature OTTLE cell recorded during the oxidation at +0.345 V *vs*. SCE of **$\{SiW_{10}\text{-}Mo_2O_4\}$** (a), at +0.345 V vs. SCE of **$\{SiW_{10}\text{-}Mo_2O_2S_2\}$** (b) or at +0.345 V vs. SCE of **$\{SiW_{10}\text{-}W_2O_2S_2\}$** (c). c = 0.1 mM in DMF + 0.1 M $LiClO_4$. Full line: before oxidation, dotted red line: after oxidation.

Computational study

Description of the electronic structure and the associated features by means of computational techniques has been largely beneficial in the comprehension of POM chemistry.[46] In this section we complement the experimental data with DFT calculations on γ-$[SiW_{10}(M_2O_2E_2)]^{n-}$ compounds in three different oxidation states, characterized by *n* = 4, 6 and 8 associated to the fully oxidized, the 2e-reduced (starting compounds) and the 4e-reduced states, respectively, owing to the number of metallic valence electrons. We aim at giving completeness to the experimental characterization as well as explaining some of the intricacies of their redox chemistry.

The main results are summarized in Table 2, which shows geometrical parameters relative to the $M_2O_2E_2$ region, orbital energies and relative molecular energies. We first put the focus on the geometry and the electronic structure of the fully oxidized form (*n* = 4). The related data can be found in the 2nd and 3rd columns of Table 2. If one focuses in the rhomb-like M_2E_2 moiety, the main difference between oxidized forms 1 and 2 is a concerted M-M lengthening/E-E shortening and *vice-versa*, as represented in the scheme 2.

Oxidized form 1 Oxidized form 2

Scheme 2

The main associated electronic difference between them is that form 1 is characterized by a closed-shell singlet ground state, whereas optimized form 2 features a triplet ground state. The highest occupied molecular orbital (HOMO) and the lowest unoccupied molecular orbital (LUMO) energies for each species are listed in Table 2.

The M-M distances are shorter in oxidized form 1 than in form 2 for all compounds. However, both forms are not interchangeable by energetic reasons since form 2 is above form 1 by more than 2 eV in Mo_2O_2 and W_2S_2 and by 0.43 eV in Mo_2S_2. So, we discard the existence of E-E bonding (E = O, S) in oxidized γ-$[SiW_{10}(M_2O_2E_2)]^{4-}$ compounds. At this stage, the metal-metal interaction in the $M_2O_2E_2$ region is destabilizing by the M^{VI}-M^{VI} repulsive electrostatic interaction, which tends to put them as far apart as possible from one another. The computed distances are 3.022, 3.748 and 3.665 Å for Mo_2O_2, Mo_2S_2 and W_2S_2, respectively, in line with previous DFT calculations that proved that the M^{VI}-M^{VI} interactions in *γ*, *δ* and *ε* Keggin isomers are destabilizing.[47] Comparatively, the γ-$[SiW_{10}(M_2O_2E_2)]^{6-}$ system features important structural differences. The two additional electrons are localized in the $M_2O_2E_2$ region, reducing the formal oxidation state of M from VI to V. In the *γ*-isomer of the Keggin structure it involves a strong structural rearrangement that entails M-M shortening and E-E lengthening, responding to the energetically favorable occupation of a bonding orbital directly associated with M-M bond formation, shown in Figure 7, which remained empty in the *electron-free* γ-$[SiW_{10}(M_2O_2E_2)]^{4-}$ form. The M-M distances shorten as much as 0.43 Å in Mo_2O_2, 0.85 Å in Mo_2S_2 and 0.80 Å in W_2S_2. Concomitantly, the two E atoms move away by 0.4 to 0.6 Å in this family. An enhancement of the bonding character of the occupied orbital is also observed due to the M-M distance shortening. Given that the occupied bonding orbital has no E-E antibonding character, the E-E separation must arise from relaxation within the rhomb-like moiety as the M-M bond is formed. It is worth mentioning that, due to the size of O and S ligands, E-E distances are much longer in $M_2O_2S_2$ than in M_2O_4.

The structures reduced with four electrons, γ-$[SiW_{10}(M_2O_2E_2)]^{8-}$, are structurally very similar to their 2-electron partners, as can be seen from the two rightmost columns of Table 2. We only notice a slight increase of the M-M and E-E distances in the $M_2O_2E_2$ region. The rest of the Keggin structure experiences small albeit generalized structural variations with W-O distances changing no more than 0.06 Å. Owing to the fact that the HOMO is delocalized over the W_{10} region and has a very marginal W-O antibonding character (see Figure 7), we attribute these minor changes to a molecular expansion, electrostatic in nature, as the overall negative charge increases upon reduction.

From the DFT-computed molecular energies, listed in Table 2, we extracted redox energies, which can be compared with electrochemical measurements presented in a previous section. To analyze the redox properties from computational results we take the γ-$[SiW_{10}(M_2O_2E_2)]^{6-}$ as the reference system. The two relevant processes are:

$$\gamma\text{-}[SiW_{10}(M_2O_2E_2)]^{6-} \rightarrow \gamma\text{-}[SiW_{10}(M_2O_2E_2)]^{4-} + 2e^- \quad \text{oxidation}$$
$$\gamma\text{-}[SiW_{10}(M_2O_2E_2)]^{6-} + 2e^- \rightarrow \gamma\text{-}[SiW_{10}(M_2O_2E_2)]^{8-} \quad \text{reduction}$$

with associated oxidation and reduction energies (OE and RE, respectively) listed in Table 3. We must take into consideration that each redox process involves two electrons. However, in the present section, the main discussion and comparison of OEs and REs is *per electron*, that is, the energy values arising from the $2e^-$-redox processes are divided by 2.

Firstly, we observe that oxidation of the $\{M_2O_2(E_2)\}^{2+}$ cores is an unfavorable process owing to the positive energies obtained. In fact, such an electron loss produces the cleavage of a covalent M-M bond, explaining that it is not spontaneous, accordingly to the experimental data. The computed energy cost per electron is +4.593 eV for $\{Mo_2O_2(S_2)\}^{2+}$, +4.198 eV for $\{Mo_2O_2(O_2)\}^{2+}$ and +4.005 eV for $\{W_2O_2(S_2)\}^{2+}$. The relative OEs in the same order are +0.193 and +0.588 eV with respect to the reference value ($W_2O_2S_2$), as shown in the table 3, in good agreement with the experimental values (+0.110 and +0.580 eV, respectively). The calculated molecular orbitals clearly explain this trend, since the $\{W_2O_2S_2\}$ structure has the HOMO at –4.91 eV, whereas the HOMOs of $\{Mo_2O_2(O_2)\}$ and $\{Mo_2O_2(S_2)\}$ are found at –5.14 eV and –5.44 eV. Since the HOMO in the $\{M_2O_2(E_2)\}^{6-}$ species has M-M bonding nature, it is entirely reasonable that M = W features the highest HOMO, and M = Mo the lowest.

The γ-$[SiW_{10}(M_2O_2E_2)]^{6-}$ + 2e → γ–$[SiW_{10}(M_2O_2E_2)]^{8-}$ process is energetically very similar within this series of compounds. As can be seen from the last row in Table 3, the three REs per electron are found within a small energy range of 63 meV. The reason is that the orbital that accepts the two electrons, the HOMO in the 4e-reduced form, has the same character and roughly the same energy (–2.61 eV in M = Mo, –2.67 eV in M = W) in all the species with no contribution from the $\{M_2O_2(E_2)\}$ region (see Figure 7). This is in quite good agreement with the superimposed reduction waves observed in the CV (see Figure 2), although $\{Mo_2O_2(O_2)\}$ features a less negative reduction potential, a fact that was not reproduced by present DFT calculations.

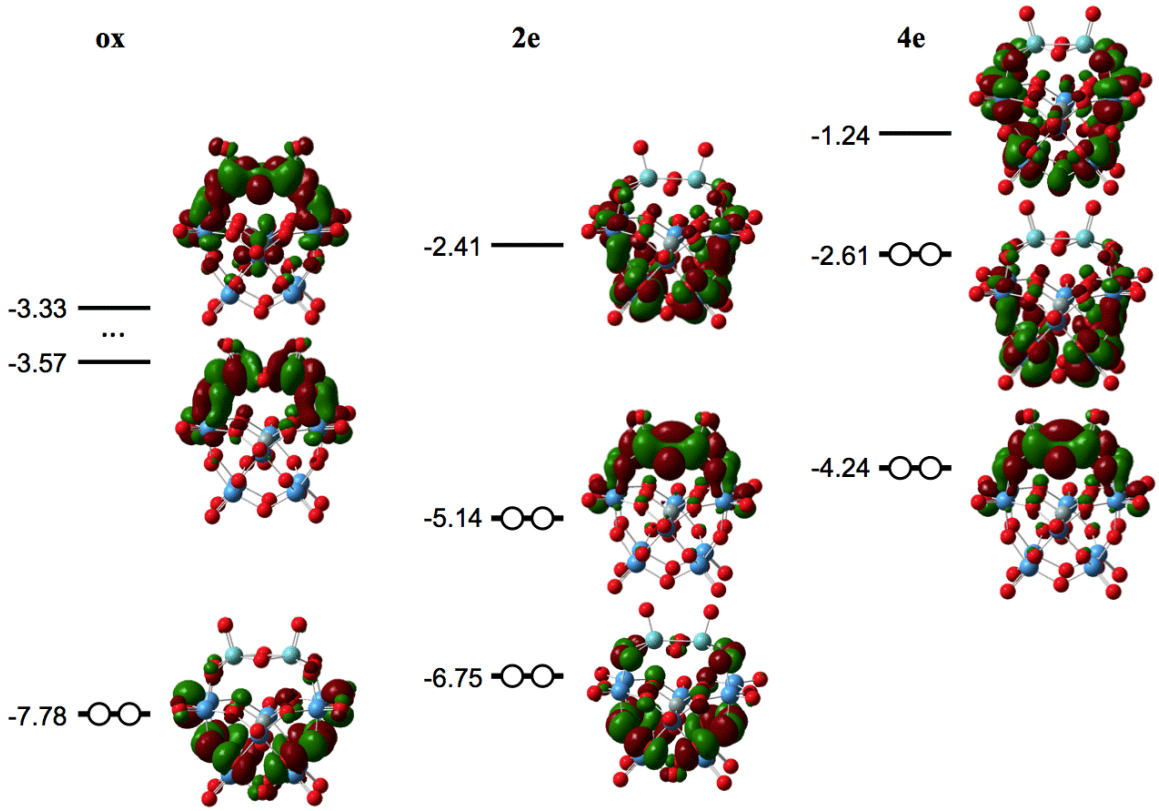

Figure 7. Molecular orbitals and associated energies (in eV) computed for $\{Mo_2O_2(O_2)\}$ with different number of electrons. Qualitatively similar features are observed for compounds $\{Mo_2O_2(S_2)\}$ and $\{W_2O_2(S_2)\}$ (see Table 2 for orbital energies).

Table 2. Relative DFT energy values (eV), relevant interatomic distances (Å) and angles (°) and molecular orbital energies in eV computed in solution for γ-$[SiW_{10}(M_2O_2E_2)]^{n-}$ compounds.

Fragment $M_2O_2E_2$		$[M^{VI}{}_2O_2(E_2)]^{4-}$	$[M^{V}{}_2O_2(E\text{-}E)]^{4-}$	$[M^{V}{}_2O_2(E_2)]^{6-}$	$[M^{V}{}_2O_2(E_2)2e]^{8-}$
Mo_2O_4	*d*(Mo-Mo)	3.022	3.383	2.592	2.605
	d(E-E)	2.400	2.101	2.805	2.807
	M-E-M angle	102.9	116.2	84.4	84.7
	HOMO	–7.78	–5.20/–7.69[a]	–5.14	–2.61
	LUMO	–3.57	–3.81/–4.91[a]	–2.41	–1.24
	Energy	0.0	+2.222	–8.397	–13.442
$Mo_2O_2S_2$	*d*(Mo-Mo)	3.748	4.075	2.895	2.927
	d(E-E)	3.092	2.136	3.678	3.690
	M-E-M angle	100.6	102.2	76.4	76.8
	HOMO	–6.12	–5.79/–7.03[a]	–5.44	–2.61
	LUMO	–3.79	–3.32/–3.29[a]	–2.38	–1.27
	Energy	0.0	+0.435	–9.186	–14.196
$W_2O_2S_2$	*d*(W-W)	3.665	4.005	2.867	2.893
	d(E-E)	3.157	2.165	3.730	3.753
	M-E-M angle	98.0	101.7	75.1	75.2
	HOMO	–6.15	–4.48/–7.40[a]	–4.91	–2.67
	LUMO	–3.56	–3.26/–3.23[a]	–2.45	–1.25
	Energy	0.0	+2.327	–8.009	–13.146

[a] Alpha/beta orbital energies, respectively.

Table 3. Oxidation and reduction energies[a] (OE and RE) computed for γ-$[SiW_{10}(M_2O_2E_2)]^{6-}$ compounds.

Redox process[b]		$\{Mo_2O_2(O_2)\}$	$\{Mo_2O_2(S_2)\}$	$\{W_2O_2(S_2)\}$
6- → 4- + 2e	OE (*total*)	+8.397	+9.186	+8.009
	OE (*per electron*)	+4.198	+4.593	+4.005
	Relative OE(*per electron*) [c]	+0.193	+0.588	0.000
6- + 2e → 8-	RE (*total*)	–5.045	–5.010	–5.137
	RE (*per electron*)	–2.522	–2.505	–2.568
	Relative RE(*per electron*) [c]	–0.017	0.000	–0.063

[a] Values in eV. [b] 4-, 6- and 8- represent the fully oxidized, 2e-reduced and 4e-reduced species. [c] Increments with respect to the indicated reference value.

Experimental

Chemicals

Chemicals purchased from Aldrich Chemicals or Acros Chemicals are used without further purification. All solvents were of reagent grade quality and used without further purification. Dimethylformamide (DMF) was purchased from Sigma-Aldrich (anhydrous, purity 99.8 %) and $LiClO_4$ from Aldrich (purity 99.99 %). The three compounds $Cs_6[SiW_{10}O_{36}(Mo_2O_2S_2)].6H_2O$ (noted **$\{SiW_{10}$-$Mo_2O_2S_2\}$**), $Cs_6[SiW_{10}O_{36}(Mo_2O_4)].6H_2O$ (noted **$\{SiW_{10}$-$Mo_2O_4\}$**) and $Cs_{4.7}K_{1.3}[SiW_{10}O_{36}(W_2O_2S_2)].7H_2O$ (noted **$\{SiW_{10}$-$W_2O_2S_2\}$**) were prepared as previously described[41, 42] and characterized by usual routine methods (FT-IR, EDX, TGA). The tetrabutylammonium salt $(NBu_4)_4H_2[SiW_{10}O_{36}(Mo_2O_2S_2)].2H_2O$ was prepared by addition of an excess of NBu_4Br to an aqueous solution of $Cs_6[SiW_{10}O_{36}(Mo_2O_2S_2)].6H_2O$ in HCl 0.5 M. The compound denoted **TBA-$\{SiW_{10}$-$Mo_2O_2S_2\}$** was isolated by filtration and characterized by elemental analysis (C, H, N, S), EDX, TGA and ^{29}Si and ^{183}W NMR (see Supporting Information).

Physical methods

Fourier Transform Infrared (FT-IR). Fourier Transform Infrared (FT-IR) spectra were recorded on a 6700 FT-IR Nicolet spectrophotometer, using diamond ATR technique. The spectra were recorded on non-diluted compounds in the range 400-4000 cm^{-1}. ATR correction was applied. **EDX** measurements were performed on a JEOL JSM 5800LV apparatus. **Elemental analyses (C, H, N, S)** were carried out by the analytical service of the CNRS at Gif sur Yvette, France. **NMR** solution spectra were recorded at 25 °C. ^{29}Si NMR were measured with a Bruker Avance 400 MHz spectrometer equipped with a 5 mm BBI probe head and operated at a magnetic field strength of 9.4 T. The ^{183}W NMR spectra were measured on a Bruker Avance 500 spectrometer at a resonance frequency of 20.8 MHz equipped with a specific low-gamma nuclei 10 mm probe head. Chemical oxidation of **TBA-$\{SiW_{10}$-$Mo_2O_2S_2\}$** by Br_2 was attempted by mixing a DMF solution of **TBA-$\{SiW_{10}$-$Mo_2O_2S_2\}$** (1.3 g in 0.75 mL of deuterated DMF + 0.5 mL of DMF) with one equivalent of a solution of Br_2 0.3 M in CH_3CN. The ^{29}Si and the ^{183}W NMR spectra are recorded after one night of reaction.

Electrochemical and Spectroelectrochemical measurements. Voltammetric data were recorded with a standard three-electrode system using a PARSTAT 2273 potentiostat. The electrolyte was DMF containing 0.1 mol L^{-1} of $LiClO_4$. Glassy carbon electrode (ø 3 mm) was used as working electrode, and a platinum wire as auxiliary electrode. The reference electrode was the saturated calomel electrode that was electrically connected to the solution by a junction bridge filled with electrolyte. The solutions were deaerated thoroughly for at least 30 minutes with pure argon and kept under a positive pressure of this gas during the experiments.

UV-Vis-NIR and FTIR spectroelectrochemical experiments were performed with an optically transparent thin-layer electrochemical (OTTLE) cell (University of Reading UK, Hartl, F.) equipped with a Pt grid working electrode and CaF_2 or KBr optical windows.[48] UV-Vis-NIR spectroelectrochemical analyses were carried out with a Zeiss MCS 601 UV–Vis–NIR diode array spectrometer. FTIR spectroelectrochemical measurements were carried out with a Brucker Vetex 80V spectrometer at 2 cm^{-1} resolution (32 scans). Spectrophotometric analyses of the films were conducted using a 0.1 M solution of $LiClO_4$ in DMF.

DFT Calculations

Full geometry optimizations have been carried out for all the compounds in the three different electronic configurations described in the text. For that purpose, we utilized the Gaussian suite of programs. This package applies gaussian-type functions to describe atomic orbitals. The valence shell electrons of all atoms were described by double-zeta basis sets, supplemented with extra polarization functions (d for oxygen, f for Mo and W) except for the heteroatom (Si). The internal electrons of Si, Mo and W are approximated to a pseudopotential of the Los Alamos National Laboratory (LANL2) type. We used the B3LYP functional[49, 50] in combination with the PCM solvation model[51] to describe the stabilizing effects of the surrounding solvent molecules. Including the solvent effects to analyze compounds with different molecular charge is a must since the gas phase approximation is not a realistic one if redox processes (species with different molecular charges) are involved. The triplet states were obtained using the unrestricted formalism.

Conclusions

In this paper, we studied the electrochemical behavior of three isoelectronic compounds $[SiW_{10}O_{36}(M_2O_2E_2)]^{6-}$ (M = Mo or W; E = S or O) in DMF medium. Their electrochemical properties were studied with the support of spectro-electrochemical studies, DFT calculations and NMR studies. It allowed demonstrating that for the

three POMs, the reduction is centered on the SiW_{10} moiety with a significant effect of the nature of the $(M_2O_2E_2)^{2+}$ core on the reduction potential of the W^{VI} centers of the POM. We also evidenced that the oxidation process focuses on the $(M_2O_2E_2)^{2+}$ core. This process is centered on the Mo(V) or W(V) atoms which are oxidized into Mo(VI) or W(VI) concomitantly with the M-M bond cleavage. Interestingly, this process appears reversible in DMF but slow in the case of $\{SiW_{10}\text{-}Mo_2O_4\}$ and $\{SiW_{10}\text{-}W_2O_2S_2\}$ and relatively fast for $\{SiW_{10}\text{-}Mo_2O_2S_2\}$. Concerning the sulfurated compounds, especially $[SiW_{10}O_{36}(Mo_2O_2S_2)]^{6-}$, coulometry experiments associated to DFT and NMR studies evidenced that the oxidation of bridging sulfides can also occur thus leading to the fully oxidized $[SiW_{10}O_{36}(Mo_2O_4)]^{4-}$ compound. This paper brings new insights into the electrochemistry of S-containing POMs in non-aqueous medium such as DMF. Our work is now focused on similar studies in aqueous medium in which pH-dependency is also expected. Such a medium allowed also envisioning applications for electro-catalysis or electro-analysis, which will be discussed in a future work.

Conflicts of interest

There are no conflicts to declare.

Acknowledgements

We are grateful to the Centre National de la Recherche Scientifique (CNRS), the Ministère de l'Enseignement Supérieur, de la Recherche et de l'Innovation (MESRI), the University of Versailles and the Université de Strasbourg for their financial support. XL also thanks the national project CTQ2014-52774-P from the Ministry of Economy, Industry and Competitivity of Spain. This work is supported by the French National Research Agency (ANR) under the contract POMEAH•ANR-08-JCJC-0097 and by the C'Nano "Ile de France" through the project ECOPOMs 2009. LR thanks also the IDEX Attractivité program of the Université de Strasbourg for this support as well Oversea Study Program of the CSC for the PhD. grant of Dr. Zang Dejin.

Notes and references

1. C. G. Lin, G. D. Fura, Y. Long, W. M. Xuan and Y. F. Song, *Inorg. Chem. Front.*, 2017, **4**, 789-794.
2. G. Izzet, B. Abecassis, D. Brouri, M. Piot, B. Matt, S. A. Serapian, C. Bo and A. Proust, *J. Am. Chem. Soc.*, 2016, **138**, 5093-5099.
3. Y. Zhu, P. C. Yin, F. P. Xiao, D. Li, E. Bitterlich, Z. C. Xiao, J. Zhang, J. Hao, T. B. Liu, Y. Wang and Y. G. Wei, *J. Am. Chem. Soc.*, 2013, **135**, 17155-17160.
4. B. Hasenknopf, *Front. Biosci.*, 2005, **10**, 275-287.
5. T. Yamase, *J. Mater. Chem.*, 2005, **15**, 4773-4782.
6. W. Salomon, Y. H. Lan, E. Riviere, S. Yang, C. Roch-Marchal, A. Dolbecq, C. Simonnet-Jegat, N. Steunou, N. Leclerc-Laronze, L. Ruhlmann, T. Mallah, W. Wernsdorfer and P. Mialane, *Chem.-Eur. J.*, 2016, **22**, 6564-6574.
7. G. Charron, A. Giusti, S. Mazerat, P. Mialane, A. Gloter, F. Miserque, B. Keita, L. Nadjo, A. Filoramo, E. Riviere, W. Wernsdorfer, V. Huc, J. P. Bourgoin and T. Mallah, *Nanoscale*, 2010, **2**, 139-144.
8. J. W. Vickers, H. J. Lv, J. M. Sumliner, G. B. Zhu, Z. Luo, D. G. Musaev, Y. V. Geletii and C. L. Hill, *J. Am. Chem. Soc.*, 2013, **135**, 14110-14118.
9. B. B. Sarma and R. Neumann, *Nat. Commun.*, 2014, **5**, 4621
10. M. Natali, M. Orlandi, S. Berardi, S. Campagna, M. Bonchio, A. Sartorel and F. Scandola, *Inorg. Chem.*, 2012, **51**, 7324-7331.
11. B. Keita and L. Nadjo, *J. Mol. Catal. A-Chem.*, 2007, **262**, 190-215.
12. M. Girardi, S. Blanchard, S. Griveau, P. Simon, M. Fontecave, F. Bedioui and A. Proust, *Eur. J. Inorg. Chem.*, 2015, 3642-3648.
13. R. J. Liu, G. J. Zhang, H. B. Cao, S. J. Zhang, Y. B. Xie, A. Haider, U. Kortz, B. H. Chen, N. S. Dalal, Y. S. Zhao, L. J. Zhi, C. X. Wu, L. K. Yan, Z. M. Su and B. Keita, *Energy Environ. Sci.*, 2016, **9**, 1012-1023.
14. B. Nohra, H. El Moll, L. M. R. Albelo, P. Mialane, J. Marrot, C. Mellot-Draznieks, M. O'Keeffe, R. N. Biboum, J. Lemaire, B. Keita, L. Nadjo and A. Dolbecq, *J. Am. Chem. Soc.*, 2011, **133**, 13363-13374.
15. B. Keita, U. Kortz, L. R. B. Holzle, S. Brown and L. Nadjo, *Langmuir*, 2007, **23**, 9531-9534.
16. S. S. Mal, M. H. Dickman, U. Kortz, A. M. Todea, A. Merca, H. Bogge, T. Glaser, A. Muller, S. Nellutla, N. Kaur, J. van Tol, N. S. Dalal, B. Keita and L. Nadjo, *Chem.-Eur. J.*, 2008, **14**, 1186-1195.
17. O. Oms, S. Yang, W. Salomon, J. Marrot, A. Dolbecq, E. Riviere, A. Bonnefont, L. Ruhlmann and P. Mialane, *Inorg. Chem.*, 2016, **55**, 1551-1561.
18. L. M. Rodríguez-Albelo, A. R. Ruiz-Salvador, A. Sampieri, D. W. Lewis, A. Gómez, B. Nohra, P. Mialane, J. Marrot, F. Secheresse, C. Mellot-Draznieks, R. N. Biboum, B. Keita, L. Nadjo and A. Dolbecq, *J. Am. Chem. Soc.*, 2009, **131**, 16078-16087.
19. Y. C. Li, W. F. Bu, L. X. Wu and C. Q. Sun, *Sens. Actuator B-Chem.*, 2005, **107**, 921-928.
20. J. Zuo, N. Gao, Z. Yu, L. Kang, K. P. O'Halloran, H. Pang, Z. Zhang and H. Ma, *J. Electroanal. Chem.*, 2015, **751**, 111-118.
21. S. Zhang, P. He, W. Lei and G. Zhang, *J. Electroanal. Chem.*, 2014, **724**, 29-35.
22. H. Wang, S. Hamanaka, Y. Nishimoto, S. Irle, T. Yokoyama, H. Yoshikawa and K. Awaga, *J. Am. Chem. Soc.*, 2012, **134**, 4918-4924.
23. Y. Nishimoto, D. Yokogawa, H. Yoshikawa, K. Awaga and S. Irle, *J. Am. Chem. Soc.*, 2014, **136**, 9042-9052.
24. T. Shibahara, *Coord. Chem. Rev.*, 1993, **123**, 73-147.
25. C. Pickett, S. Kumar, P. Vella and J. Zubieta, *Inorg. Chem.*, 1982, **21**, 908-916.
26. J. Marrot, M. A. Pilette, M. Haouas, S. Floquet, F. Taulelle, X. Lopez, J. M. Poblet and E. Cadot, *J. Am. Chem. Soc.*, 2012, **134**, 1724-1737.
27. E. Cadot, M. N. Sokolov, V. P. Fedin, C. Simonnet-Jegat, S. Floquet and F. Sécheresse, *Chem. Soc. Rev.*, 2012, **41**, 7335-7353.
28. S. Duval, M. A. Pilette, J. Marrot, C. Simonnet-Jegat, M. Sokolov and E. Cadot, *Chem.-Eur. J.*, 2008, **14**, 3457-3466.
29. V. S. Korenev, A. G. Boulay, M. Haouas, F. Bannani, V. P. Fedin, M. N. Sokolov, E. Terazzi, S. Garai, A. Müller, F. Taulelle, J. Marrot, N. Leclerc, S. Floquet and E. Cadot, *Chem.-Eur. J.*, 2014, **20**, 3097-3105.
30. V. R. Ott, D. S. Swieter and F. A. Schultz, *Inorg. Chem.*, 1977, **16**, 2538-2545.
31. F. A. Schultz, V. R. Ott, D. S. Rolison, D. C. Bravard, J. W. McDonald and W. E. Newton, *Inorg. Chem.*, 1978, **17**, 1758-1765.

32. A. Hijazi, J. C. Kemmegne-Mbouguen, S. Floquet, J. Marrot, J. Fize, V. Artero, O. David, E. Magnier, B. Pegot and E. Cadot, *Dalton Trans.*, 2013, **42**, 4848-4858.
33. H. El Moll, J. C. Kemmegne-Mbouguen, M. Haouas, F. Taulelle, J. Marrot, E. Cadot, P. Mialane, S. Floquet and A. Dolbecq, *Dalton Trans.*, 2012, **41**, 9955-9963.
34. A. Hijazi, J. C. Kemmegne-Mbouguen, S. Floquet, J. Marrot, C. R. Mayer, V. Artero and E. Cadot, *Inorg. Chem.*, 2011, **50**, 9031-9038.
35. S. Duval, S. Floquet, C. Simonnet-Jegat, J. Marrot, R. N. Biboum, B. Keita, L. Nadjo, M. Haouas, F. Taulelle and E. Cadot, *J. Am. Chem. Soc.*, 2010, **132**, 2069-2077.
36. B. Keita, S. Floquet, J. F. Lemonnier, E. Cadot, A. Kachmar, M. Benard, M. M. Rohmer and L. Nadjo, *J. Phys. Chem. C*, 2008, **112**, 1109-1114.
37. T. Shibahara, M. Yamasaki, G. Sakane, K. Minami, T. Yabuki and A. Ichimura, *Inorg. Chem.*, 1992, **31**, 640-647.
38. A. B. Laursen, S. Kegnaes, S. Dahl and I. Chorkendorff, *Energy Environ. Sci.*, 2012, **5**, 5577-5591.
39. Y. D. Hou, B. L. Abrams, P. C. K. Vesborg, M. E. Bjorketun, K. Herbst, L. Bech, A. M. Setti, C. D. Damsgaard, T. Pedersen, O. Hansen, J. Rossmeisl, S. Dahl, J. K. Norskov and I. Chorkendorff, *Nat. Mater.*, 2011, **10**, 434-438.
40. J. Kristensen, J. D. Zhang, I. Chorkendorff, J. Ulstrup and B. L. Ooi, *Dalton Trans.*, 2006, 3985-3990.
41. A. Tézé, E. Cadot, V. Béreau and G. Hervé, *Inorg. Chem.*, 2001, **40**, 2000-2004.
42. E. Cadot, V. Béreau, B. Marg, S. Halut and F. Sécheresse, *Inorg. Chem.*, 1996, **35**, 3099-3106.
43. T. Shibahara, M. Yamasaki, T. Watase and A. Ichimura, *Inorg. Chem.*, 1994, **33**, 292-301.
44. R. Thouvenot, M. Fournier, R. Franck and C. Rocchicciolideltcheff, *Inorg. Chem.*, 1984, **23**, 598-605.
45. C. Rocchicciolideltcheff, M. Fournier, R. Franck and R. Thouvenot, *Inorg. Chem.*, 1983, **22**, 207-216.
46. X. López, J. J. Carbó, C. Bo and J. M. Poblet, *Chem. Soc. Rev.*, 2012, **41**, 7537-7571.
47. X. López and J. M. Poblet, *Inorg. Chem.*, 2004, **43**, 6863-6865.
48. M. Krejcik, M. Danek and F. Hartl, *J. Electroanal. Chem.*, 1991, **317**, 179-187.
49. P. J. Stephens, F. J. Devlin, C. F. Chabalowski and M. J. Frisch, *J. Phys. Chem.*, 1994, **98**, 11623-11627.
50. C. T. Lee, W. T. Yang and R. G. Parr, *Phys. Rev. B*, 1988, **37**, 785-789.
51. S. Miertus, E. Scrocco and J. Tomasi, *Chem. Phys.*, 1981, **55**, 117-129.